Journal of Alloys and Compounds 519 (2012) 85–91

Contents lists available at SciVerse ScienceDirect

Journal of Alloys and Compounds

journal homepage: www.elsevier.com/locate/jallcom

Crystal structures and magnetic properties of $R_2PbSi_2S_8$ (R = Y, Ce, Pr, Nd, Sm, Gd, Tb, Dy, Ho), $R_2PbSi_2Se_8$ (R = La, Ce, Pr, Nd, Sm, Gd) and $R_2PbGe_2S_8$ (R = Ce, Pr) compounds

M. Daszkiewicz [a], O.V. Marchuk [b], L.D. Gulay [c], D. Kaczorowski [a,*]

[a] Institute of Low Temperature and Structure Research, Polish Academy of Sciences, P.O. Box 1410, 50-950 Wrocław, Poland
[b] Department of Inorganic and Physical Chemistry, Volyn National University, Voli Ave 13, 43009 Lutsk, Ukraine
[c] Department of Ecology and Protection of Environment, Volyn National University, Voli Ave 13, 43009 Lutsk, Ukraine

ARTICLE INFO

Article history:
Received 22 November 2011
Received in revised form
17 December 2011
Accepted 19 December 2011
Available online 3 January 2012

Keywords:
Rare earth compounds
Chalcogenides
Crystal structures
X-ray single crystal diffraction
X-ray powder diffraction
Magnetic properties

ABSTRACT

The crystal structures of several novel quaternary compounds $R_2PbSi_2S_8$ (R = Y, Ce, Pr, Nd, Sm, Gd, Tb, Dy, Ho), $R_2PbSi_2Se_8$ (R = La, Ce, Pr, Nd, Sm, Gd) and $R_2PbGe_2S_8$ (R = Ce, Pr) have been determined by means of single-crystal and powder X-ray diffraction. All these phases crystallize with hexagonal unit cells of the $La_2PbSi_2S_8$ type (space group *R*-3*c*, Pearson symbol *hR*78), in which rare-earth and lead atoms are statistically distributed over centers of bi-capped trigonal prisms made by chalcogen atoms. The magnetic properties of $R_2PbSi_2S_8$ and $R_2PbSi_2Se_8$ with R = La, Ce, Pr and Sm have been studied in wide temperature and magnetic field ranges. The La-based materials are weakly diamagnetic, whereas all the other compounds exhibit strongly temperature dependent paramagnetic behaviour due to the presence of well localized magnetic moments of trivalent rare-earth ions.

1. Introduction

Designing new functional materials with increasingly complex compositions has become a primary direction in modern science and technology. Complex rare-earth-based chalcogenides are interesting due to their specific thermal, electrical, magnetic and optical properties [1,2]. For example, some chalcogenide materials found their specific applications in the field of infrared and nonlinear optics. Obviously, further systematic investigation of various chalcogenide systems is an important way towards finding materials with tailored physical properties [3].

Recently, we have established the formation of a novel sulphide $La_2PbSi_2S_8$ that crystallizes with its own crystal structure type of the space group *R*-3*c* [4]. In the present paper we demonstrate the existence of several isostructural compounds $R_2PbSi_2S_8$ (R = Y, Ce, Pr, Nd, Sm, Gd, Tb, Dy, Ho), $R_2PbGe_2S_8$ (R = Ce, Pr) and $R_2PbSi_2Se_8$ (R = La, Ce, Pr, Nd, Sm, Gd). For some of these phases we report on their low-temperature magnetic properties.

2. Experimental details

Powder samples with the overall nominal composition $R_2PbZ_2X_8$ (R = rare earth; Z = Si, Ge; X = S, Se) were prepared by sintering the elemental constituents of the purity better than 99.9 wt.% in evacuated quartz tubes. The syntheses were carried out in a tube resistance furnace. The ampoules were first heated with a rate of 30 °C per hour up to 1150 °C, and then kept at this temperature for 3 h. Afterwards, the samples were cooled slowly (10 °C per hour) down to 500 °C, and annealed at this temperature for 720 h. Subsequently, the ampoules were quenched in air.

The products were checked by X-ray powder diffraction using a DRON-4-13 powder diffractometer (Cu Kα radiation, $10^\circ \leq 2\Theta \leq 100^\circ$, step scan mode with a step size of 0.05° and counting time of 10 s per data point). The phase analysis was carried out and the lattice parameters were determined using the CSD software package [5]. As a result, the formation of $R_2PbSi_2S_8$ (R = Y, Ce, Pr, Nd, Sm, Gd, Tb, Dy, Ho), $R_2PbGe_2S_8$ (R = Ce, Pr) and $R_2PbSi_2Se_8$ (R = La, Ce, Pr, Nd, Sm, Gd) has been established.

Small single crystals suitable for crystal structure investigations were selected from the $R_2PbSi_2S_8$ (R = Ce, Pr, Nd), $Ce_2PbGe_2S_8$ and $R_2PbSi_2Se_8$ (R = La, Ce, Pr, Nd) samples. The X-ray intensities data were collected on a KUMA Diffraction KM-4 four-circle diffractometer equipped with a CCD camera, using graphite-monochromatized Mo Kα radiation (λ = 0.071073 nm). The raw data were treated with the CrysAlis Data Reduction program [6] taking into account an absorption correction. The intensities of the reflections were corrected for Lorentz and polarization factors. The crystal structure was solved by Patterson methods [7] and refined by the full-matrix least-squares method using SHELXL-97 [7]. Space group *R*-3*c* was checked with the PLATON program, and no additional symmetry elements were found [8].

All the single crystals were examined on a Phillips 515 scanning electron microscope equipped with an EDAX PV 9800 spectrometer. The results confirmed

* Corresponding author.
E-mail address: D.Kaczorowski@int.pan.wroc.pl (D. Kaczorowski).

0925-8388/$ – see front matter © 2011 Elsevier B.V. All rights reserved.
doi:10.1016/j.jallcom.2011.12.097

Table 1
Crystal data and structure refinement details of the $R_2PbSi_2S_8$ (R = Ce, Pr, Nd) and $Ce_2PbGe_2S_8$ compounds.

Empirical formula	$Ce_2PbSi_2S_8$	$Pr_2PbSi_2S_8$	$Nd_2PbSi_2S_8$	$Ce_2PbGe_2S_8$
Formula weight	800.09	801.67	808.33	889.09
Space group	*R*-3*c* (No. 167)	*R*-3*c* (No. 167)	*R*-3*c* (No. 167)	*R*-3*c* (No. 167)
Unit cell dimensions	$a = 9.0030(7)$ Å $c = 26.765(3)$ Å	$a = 8.9744(7)$ Å $c = 26.640(2)$ Å	$a = 8.942(1)$ Å $c = 26.492(4)$ Å	$a = 9.0176(6)$ Å $c = 26.980(3)$ Å
Volume	1878.7(3) Å^3	1858.1(3) Å^3	1834.8(4) Å^3	1900.3(3) Å^3
Number of formula units per unit cell	6	6	6	6
Calculated density	4.243 g/cm^3	4.299 g/cm^3	4.389 g/cm^3	4.662 g/cm^3
Absorption coefficient	22.028 mm^{-1}	22.790 mm^{-1}	23.603 mm^{-1}	26.247 mm^{-1}
F(0 0 0)	2124	2136	2148	2340
Crystal colour	Red	Yellow	Red	Red
Crystal size	0.08 mm × 0.0 7 mm × 0.06 mm	0.08 mm × 0.06 mm × 0.03 mm	0.09 mm × 0.06 mm × 0.03 mm	0.07 mm × 0.03 mm × 0.03 mm
Θ range for data collection	3.02–27.48	3.03–27.41	3.05–26.90	3.01–27.48
Index ranges	$-11 \le h \le 11; -11 \le k \le 11; -32 \le l \le 34$	$-11 \le h \le 11; -11 \le k \le 11; -32 \le l \le 34;$	$-11 \le h \le 11; -11 \le k \le 11; -32 \le l \le 33$	$-11 \le h \le 11; -11 \le k \le 11; -34 \le l \le 34$
Reflections collected	4983	4828	5794	4886
Independent reflections	485 [*R*(int.) = 0.0332]	480 [*R*(int.) = 0.0522]	447 [*R*(int.) = 0.0927]	491 [*R*(int.) = 0.0739]
Refinement method	Full-matrix least-square on F^2	Full-matrix least-square on F^2	Full-matrix least-square on F^2	Full-matrix least-square on F^2
Data/restraints/parameters	485/0/21	480/0/21	447/0/21	491/0/21
Goodness-of-fit on F^2	1.582	1.200	1.231	1.138
Final *R* indices [$I > 2\sigma(I)$]	*R*1 = 0.0233, *wR*2 = 0.0414	*R*1 = 0.0315, *wR*2 = 0.0558	*R*1 = 0.0351, *wR*2 = 0.0849	*R*1 = 0.0368, *wR*2 = 0.0450
R indices (all data)	*R*1 = 0.0270, *wR*2 = 0.0420	*R*1 = 0.0398, *wR*2 = 0.0581	*R*1 = 0.0389, *wR*2 = 0.0870	*R*1 = 0.0568, *wR*2 = 0.0496
Extinction coefficient				
Largest diff. peak and hole	1.056 and −0.932 e/Å^3	1.284 and −1.411 e/Å^3	3.320 and −1.720 e/Å^3	1.536 and −1.309 e/Å^3

Table 2
Crystal data and structure refinement details of the $R_2PbSi_2Se_8$ (R = La, Ce, Pr, Nd) compounds.

Empirical formula	$La_2PbSi_2Se_8$	$Ce_2PbSi_2Se_8$	$Pr_2PbSi_2Se_8$	$Nd_2PbSi_2Se_8$
Formula weight	1172.87	1175.29	1176.87	1183.53
Space group	*R*-3*c* (No. 167)	*R*-3*c* (No. 167)	*R*-3*c* (No. 167)	*R*-3*c* (No. 167)
Unit cell dimensions	$a = 9.3984(6)$ Å $c = 28.089(3)$ Å	$a = 9.351(1)$ Å $c = 27.908(4)$ Å	$a = 9.3264(9)$ Å $c = 27.779(3)$ Å	$a = 9.2998(9)$ Å $c = 27.670(2)$ Å
Volume	2148.7(3) Å^3	2113.8(5) Å^3	2092.5(3) Å^3	2072.5(3) Å^3
Number of formula units per unit cell	6	6	6	6
Calculated density	5.438 g/cm^3	5.540 g/cm^3	5.603 g/cm^3	5.690 g/cm^3
Absorption coefficient	38.032 mm^{-1}	39.058 mm^{-1}	39.913 mm^{-1}	40.763 mm^{-1}
F(0 0 0)	2976	2988	3000	3012
Crystal colour	Red	Dark red	Red	Red
Crystal size	0.09 mm × 0.04 mm × 0.03 mm	0.06 mm × 0.05 mm × 0.04 mm	0.08 mm × 0.05 mm × 0.04 mm	0.08 mm × 0.05 mm × 0.05 mm
Θ range for data collection	3.83–27.48	2.91–27.45	3.83–27.48	2.93–27.10
Index ranges	$-12 \le h \le 12; -11 \le k \le 12; -36 \le l \le 36$	$-12 \le h \le 11; -11 \le k \le 11; -35 \le l \le 35$	$-11 \le h \le 12; -11 \le k \le 11; -35 \le l \le 36$	$-11 \le h \le 11; -11 \le k \le 11; -35 \le l \le 34$
Reflections collected	5503	5537	5287	5321
Independent reflections	551 [*R*(int.) = 0.0739]	536 [*R*(int.) = 0.0791]	535 [*R*(int.) = 0.0736]	514 [*R*(int.) = 0.1143]
Refinement method	Full-matrix least-square on F^2	Full-matrix least-square on F^2	Full-matrix least-square on F^2	Full-matrix least-square on F^2
Data/restraints/parameters	551/0/21	536/0/21	535/0/22	514/0/22
Goodness-of-fit on F^2	1.174	1.210	1.248	1.312
Final *R* indices [$I > 2\sigma(I)$]	*R*1 = 0.0416, *wR*2 = 0.0627	*R*1 = 0.0500, *wR*2 = 0.0643	*R*1 = 0.0446, *wR*2 = 0.0775	*R*1 = 0.0538, *wR*2 = 0.1112
R indices (all data)	*R*1 = 0.0563, *wR*2 = 0.0668	*R*1 = 0.0652, *wR*2 = 0.0679	*R*1 = 0.0586, *wR*2 = 0.0819	*R*1 = 0.0620, *wR*2 = 0.1148
Extinction coefficient			0.00024(3)	0.00079(9)
Largest diff. peak and hole	1.225 and −1.527 e/Å^3	1.059 and −1.020 e/Å^3	1.555 and −1.728 e/Å^3	2.103 and −2.152 e/Å^3

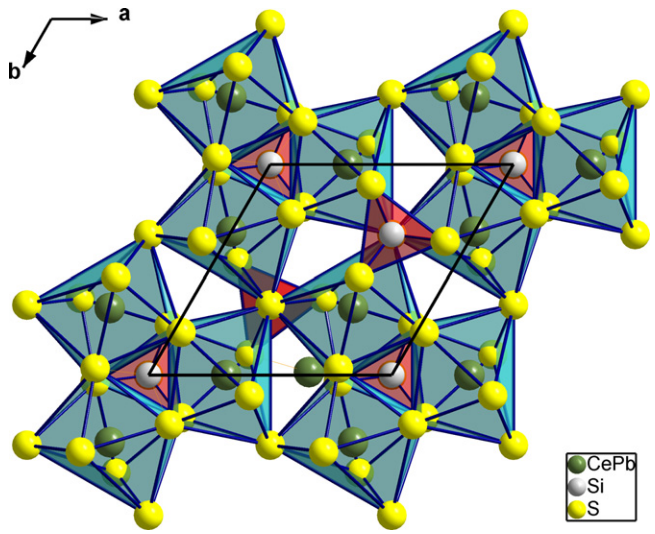

Fig. 1. Coordination polyhedra of the (2/3Ce + 1/3Pb) and Si atoms in the structure of $Ce_2PbSi_2S_8$.

homogeneous single-phase materials with the compositions equal to those revealed in the X-ray studies.

Magnetic measurements were performed in the temperature range 1.72–400 K and in applied magnetic fields to 5 T using a Quantum Design MPMS-5 superconducting quantum interface device (SQUID) magnetometer.

3. Results and discussion

3.1. Crystal structure

The crystal data and the structure refinement details for the $R_2PbSi_2S_8$ (R = Ce, Pr, Nd), $Ce_2PbGe_2S_8$ and $R_2PbSi_2Se_8$ (R = La, Ce, Pr, Nd) phases are summarized in Tables 1 and 2, whereas the refined atomic coordinates and the thermal displacement factors are given in Table 3. In accordance with the results obtained recently for $La_2PbSi_2S_8$ [4], in the unit cell of the compounds studied, there are a single site (18e) randomly occupied by a mixture of the R and Pb atoms, one position of the Si(Ge) atoms and two positions of the chalcogen atoms. The positions of the Si(Ge) and S(Se) atoms are fully occupied. For each material, treating the 18e site occupancy factor as a free parameter, it has been refined to a numerical value close to 2/3R + 1/3Pb. It is worthwhile noting that the latter composition of the statistical mixture satisfies the charge balance requirements in the $R_2PbZ_2X_8$ compounds. The relevant interatomic distances and the coordination numbers of the atoms of the statistical mixture (R + Pb) and the Si(Ge) atoms are gathered in Table 4. All the distances are close to the sums of the respective ionic radii [9].

The lattice parameters refined for the $R_2PbSi_2S_8$ (R = Y, Sm, Gd, Tb, Dy, Ho), $Pr_2PbGe_2S_8$ and $R_2PbSi_2Se_8$ (R = Sm, Gd) compounds from the X-ray powder diffraction data are listed in Table 5. They nicely correspond with the results derived for the single crystals of the other phases, hence proving their isostructural character.

Fig. 1 presents the crystal structure of the $R_2PbSi_2S_8$ (R = Y, Ce, Pr, Nd, Sm, Gd, Tb, Dy, Ho), $R_2PbGe_2S_8$ (R = Ce, Pr) and $R_2PbSi_2Se_8$ (R = La, Ce, Pr, Nd, Sm, Gd) compounds, exemplified for $Ce_2PbSi_2S_8$. Generally, the atom framework consists of $[(2/3Ce + 1/3Pb)S1_2S2_6]$ bi-capped trigonal prisms and $[SiS1_1S2_3]$ tetrahedra, which are mutually connected by corners and edges. For more details on this crystal structure the interested reader is referred to Ref. [4]. As shown in Fig. 2, the unit cell volume of the compounds studied exhibits the so-called lanthanide contraction variation when going from La to Ho, namely it systematically increases with increasing the ionic radius of the rare-earth element.

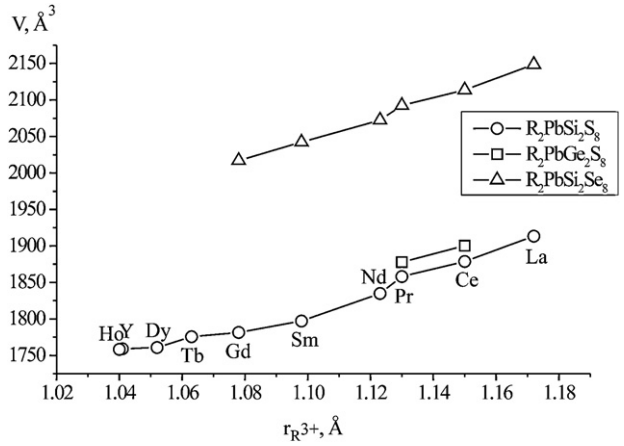

Fig. 2. The dependence of the unit cell volume of the $R_2PbSi_2S_8$ (R = Y, La, Ce, Pr, Nd, Sm, Gd, Tb, Dy, Ho), $R_2PbGe_2S_8$ (R = Ce, Pr), $R_2PbSi_2Se_8$ (R = La, Ce, Pr, Nd, Sm, Gd) compounds on the ionic radii of the rare earth elements.

3.2. Magnetic properties

The results of magnetic measurements of the $R_2PbSi_2S_8$ (R = La, Ce, Pr, Sm) compounds are summarized in Fig. 3, while those obtained for the $R_2PbSi_2Se_8$ (R = La, Ce, Pr, Sm) phases are gathered in Fig. 4. Apparently, the La-containing materials are weakly magnetic with the magnetic susceptibility being independent of temperature over extended temperature range. The upturns in $\chi(T)$ observed at low temperatures arise because of the presence of small amounts of magnetic impurities in the samples studied. Though the room-temperature susceptibility is slightly positive for $La_2PbSi_2S_8$ and negative for $La_2PbSi_2Se_8$, both materials are weak diamagnets. This conclusion can be driven from the characteristic field dependence of the magnetization measured at low temperatures (see the insets), which initially increases with increasing magnetic field, yet then starts to decrease. The negative slopes in $\sigma(H)$, seen in fields strong enough to overcome the paramagnetic contributions due to impurities, clearly manifest the intrinsic diamagnetic nature of the two compounds. The magnetic susceptibility derived from the magnetization data is equal to -4×10^{-7} emu/g for $La_2PbSi_2S_8$ and -3×10^{-7} emu/g for $La_2PbSi_2Se_8$.

In contrast to the La-based materials, which do not contain any 4f electrons, the other quaternaries investigated exhibit localized magnetism that manifests itself in strong temperature dependencies of their magnetic susceptibility. As demonstrated in Figs. 3 and 4, in wide regions below room temperature, the reciprocal susceptibility of Ce- and Pr-based chalcogenides shows a straight-line behaviour that can be approximated by the Curie–Weiss (CW) law $x = C/(T - \theta)$, where θ stands for the paramagnetic Curie temperature and the parameter C is linked to the effective magnetic moment μ_{eff} via the relation $\mu_{eff}\sqrt{8C}$. The CW parameters derived for $Ce_2PbSi_2S_8$ are $\mu_{eff} = 2.51\,\mu_B$/Ce-ion and $\theta = 38$ K and those calculated for $Ce_2PbSi_2Se_8$ are $\mu_{eff} = 2.30\,\mu_B$/Ce-ion and $\theta = 9$ K. The parameters found for $Pr_2PbSi_2S_8$ are $\mu_{eff} = 3.65\,\mu_B$/Pr-ion and $\theta = 54$ K and those for $Pr_2PbSi_2Se_8$ are $\mu_{eff} = 3.53\,\mu_B$/Pr-ion and $\theta = 39$ K. Noticeably, the experimental values of the effective magnetic moment are close to the theoretical ones calculated within the Russell–Saunders coupling scenario for free trivalent Ce and Pr ions that amount to 2.54 and 3.58 μ_B, respectively. The large positive values of the paramagnetic Curie temperature might suggest fairly strong ferromagnetic correlations between the magnetic moments carried on the rare-earth ions. However, none of the compounds orders magnetically in the temperature range studied. The distinct deviations from the CW law, observed for each

Table 3
Atomic coordinates and thermal displacement factors for the $R_2PbSi_2S_8$ (R = Ce, Pr, Nd), $Ce_2PbGe_2S_8$ and $R_2PbSi_2Se_8$ (R = La, Ce, Pr, Nd) compounds.

Atom	Position	x/a	y/b	z/c	Occupancy	$U_{eq.}$, Å^2	U_{11}	U_{22}	U_{33}	U_{23}	U_{13}	U_{12}
$Ce_2PbSi_2S_8$												
M	18*e*	0.31908(3)	0.31908(3)	1/4	2/3Ce + 1/3Pb	0.0209(1)	0.0253(1)	0.0253(1)	0.0173(1)	0.00100(6)	−0.00100(6)	0.0165(1)
Si	12*c*	0	0	0.15964(7)	1	0.0179(5)	0.0198(7)	0.0198(7)	0.013(1)	0	0	0.0099(3)
S1	12*c*	0	0	0.08028(7)	1	0.0225(4)	0.0276(7)	0.0276(7)	0.0124(9)	0	0	0.0138(3)
S2	36*f*	0.0322(1)	0.2356(1)	0.18649(5)	1	0.0241(3)	0.0251(6)	0.0294(6)	0.0224(6)	−0.0113(5)	−0.0083(5)	0.0172(5)
$Pr_2PbSi_2S_8$												
M	18*e*	0.31932(5)	0.31932(5)	1/4	2/3Pr + 1/3Pb	0.0229(1)	0.0280(2)	0.0280(2)	0.0190(3)	0.00093(8)	−0.00093(8)	0.0187(2)
Si	12*c*	0	0	0.15951(9)	1	0.0203(6)	0.022(1)	0.022(1)	0.015(1)	0	0	0.0114(5)
S1	12*c*	0	0	0.07979(9)	1	0.0255(6)	0.0318(9)	0.0318(9)	0.0130(12)	0	0	0.0159(5)
S2	36*f*	0.0324(2)	0.2365(2)	0.18656(6)	1	0.0259(4)	0.0253(9)	0.0327(9)	0.0251(8)	−0.0120(7)	−0.0088(7)	0.0186(7)
$Nd_2PbSi_2S_8$												
M	18*e*	0.31968(6)	0.31968(6)	1/4	2/3Nd + 1/3Pb	0.0244(3)	0.0300(3)	0.0300(3)	0.0203(4)	0.00089(9)	−0.00089(9)	0.0204(3)
Si	12*c*	0	0	0.15965(12)	1	0.0226(8)	0.023(1)	0.023(1)	0.021(1)	0	0	0.0116(6)
S1	12*c*	0	0	0.07988(10)	1	0.0266(7)	0.032(1)	0.032(1)	0.015(1)	0	0	0.0160(6)
S2	36*f*	0.0324(3)	0.2371(3)	0.18653(7)	1	0.0291(5)	0.028(1)	0.034(1)	0.029(1)	−0.0132(8)	−0.0091(8)	0.0197(9)
$Ce_2PbGe_2S_8$												
M	18*e*	0.32070(5)	0.32070(5)	1/4	2/3Ce + 1/3Pb	0.0246(1)	0.0293(3)	0.0293(3)	0.0213(2)	0.0009(1)	−0.0009(1)	0.0191(3)
Ge	12*c*	0	0	0.15988(4)	1	0.0211(3)	0.0235(5)	0.0235(5)	0.0163(6)	0	0	0.0118(2)
S1	12*c*	0	0	0.07782(9)	1	0.0265(8)	0.031(1)	0.031(1)	0.016(1)	0	0	0.0158(6)
S2	36*f*	0.0320(2)	0.2440(3)	0.18762(7)	1	0.0289(5)	0.027(1)	0.035(1)	0.0297(9)	−0.0142(8)	−0.0093(8)	0.0200(9)
$La_2PbSi_2Se_8$												
M	18*e*	0.31897(6)	0.31897(6)	1/4	2/3La + 1/3Pb	0.0259(2)	0.0294(3)	0.0294(3)	0.0242(3)	0.0014(1)	−0.0014(1)	0.0186(3)
Si	12*c*	0	0	0.1595(1)	1	0.0198(9)	0.021(1)	0.021(1)	0.016(2)	0	0	0.0108(7)
Se1	12*c*	0	0	0.07844(5)	1	0.0243(4)	0.0280(5)	0.0280(5)	0.0169(7)	0	0	0.0140(3)
Se2	36*f*	0.0319(1)	0.2412(1)	0.18684(3)	1	0.0283(3)	0.0285(5)	0.0328(5)	0.0278(5)	−0.0131(4)	−0.0078(4)	0.0186(4)
$Ce_2PbSi_2Se_8$												
M	18*e*	0.31929(8)	0.31929(8)	1/4	2/3Ce + 1/3Pb	0.0270(2)	0.0322(4)	0.0322(4)	0.0236(4)	0.00186(15)	−0.0018(1)	0.0212(4)
Si	12*c*	0	0	0.1593(1)	1	0.021(1)	0.022(1)	0.022(1)	0.017(2)	0	0	0.0114(8)
Se1	12*c*	0	0	0.07781(6)	1	0.0259(4)	0.0304(6)	0.0304(6)	0.0168(9)	0	0	0.0152(3)
Se2	36*f*	0.0325(1)	0.2423(1)	0.18684(4)	1	0.0291(3)	0.0283(6)	0.0350(6)	0.0284(6)	−0.0138(4)	−0.0087(4)	0.0193(5)
$Pr_2PbSi_2Se_8$												
M	18*e*	0.31926(8)	0.31926(8)	1/4	2/3Pr + 1/3Pb	0.0259(3)	0.0325(4)	0.0325(4)	0.0209(4)	0.0016(1)	−0.0016(1)	0.0224(4)
Si	12*c*	0	0	0.1593(1)	1	0.019(1)	0.021(1)	0.021(1)	0.014(2)	0	0	0.0109(8)
Se1	12*c*	0	0	0.07735(6)	1	0.0263(4)	0.0320(7)	0.0320(7)	0.0149(7)	0	0	0.0160(3)
Se2	36*f*	0.0326(1)	0.2431(1)	0.18694(4)	1	0.0284(4)	0.0288(6)	0.0358(7)	0.0264(5)	−0.0145(4)	−0.0095(4)	0.0205(5)
$Nd_2PbSi_2Se_8$												
M	18*e*	0.3191(1)	0.3191(1)	1/4	2/3Nd + 1/3Pb	0.0246(4)	0.0318(5)	0.0318(5)	0.0192(5)	0.0015(1)	−0.0015(1)	0.0226(4)
Si	12*c*	0	0	0.1592(1)	1	0.020(1)	0.022(2)	0.022(2)	0.017(3)	0	0	0.011(1)
Se1	12*c*	0	0	0.07704(7)	1	0.0258(6)	0.0326(8)	0.0326(8)	0.0123(9)	0	0	0.0163(4)
Se2	36*f*	0.0325(1)	0.2434(1)	0.18702(5)	1	0.0272(5)	0.0260(7)	0.0355(9)	0.0262(7)	−0.0159(5)	−0.0098(5)	0.0199(6)

$U_{eq.}$ is defined as one third of the trace of the orthogonalized U_{ij} tensor.
The anisotropic temperature factor exponent takes the form: $-2\pi^2[h^2a^{*2}U_{11} + \cdots + 2hka^*b^*U_{12}]$.

Table 4
Interatomic distances (in Å) and coordination numbers (C.N.) of the atoms of the statistical mixture (R + Pb) and Si (Ge) atoms in $R_2PbSi_2S_8$ (R = Ce, Pr, Nd), $Ce_2PbGe_2S_8$ and $R_2PbSi_2Se_8$ (R = La, Ce, Pr, Nd).

Atoms	$Ce_2PbSi_2S_8$	$Pr_2PbSi_2S_8$	$Nd_2PbSi_2S_8$	$Ce_2PbGe_2S_8$	$La_2PbSi_2Se_8$	$Ce_2PbSi_2Se_8$	$Pr_2PbSi_2Se_8$	$Nd_2PbSi_2Se_8$	C.N.	
R + Pb	—2S(Se)2	2.860(1)	2.850(1)	2.841(1)	2.878(1)	2.997(1)	2.980(1)	2.969(1)	2.959(1)	8
	—1S(Se)2	2.989(1)	2.975(1)	2.956(2)	3.008(1)	3.125(1)	3.103(1)	3.089(1)	3.079(1)	
	—1S(Se)2	2.989(1)	2.975(1)	2.956(2)	3.008(1)	3.125(1)	3.103(1)	3.089(1)	3.079(1)	
	—2S(Se)1	3.0682(3)	3.0577(3)	3.0451(4)	3.0680(4)	3.2053(4)	3.1887(6)	3.1808(5)	3.1728(6)	
	—2S(Se)2	3.268(1)	3.259(1)	3.250(2)	3.285(2)	3.419(1)	3.407(1)	3.397(1)	3.384(1)	
Si(Ge)	—3S(Se)2	2.118(1)	2.118(1)	2.115(2)	2.202(1)	2.267(1)	2.264(1)	2.265(1)	2.264(2)	4
	—1S(Se)1	2.124(3)	2.124(3)	2.113(4)	2.214(3)	2.277(4)	2.276(4)	2.277(4)	2.275(6)	

material below about 200 K, most likely originate from gradual depopulation of excited crystalline electric field states with decreasing temperature. The absence of any long-range magnetic ordering in $Ce_2PbSi_2S_8$, $Ce_2PbSi_2Se_8$, $Pr_2PbSi_2S_8$ and $Pr_2PbSi_2Se_8$ is corroborated by the featureless low-temperature variations of their magnetic susceptibility (see the upper insets in the respective panels in Figs. 3 and 4), as well as by the field-dependent magnetization data taken at 1.72 K (see the lower insets), which exhibit paramagnetic Brillouin-like character. The magnetization measured at this temperature in the strongest field available in our experiment, i.e. $\mu_0 H = 5$ T, corresponds to the magnetic moment of 1.4, 1.0, 2.5 and 0.7 μ_B per rare-earth ion for $Ce_2PbSi_2S_8$, $Ce_2PbSi_2Se_8$, $Pr_2PbSi_2S_8$ and $Pr_2PbSi_2Se_8$, respectively. It is worthwhile noting that these values are systematically much larger in the sulphides than in the selenides, yet still for each compound distinctly smaller than the theoretical spontaneous moments of free Ce^{3+} and Pr^{3+} ions, which are equal to 2.14 and 3.2 μ_B, respectively. The observed reduction

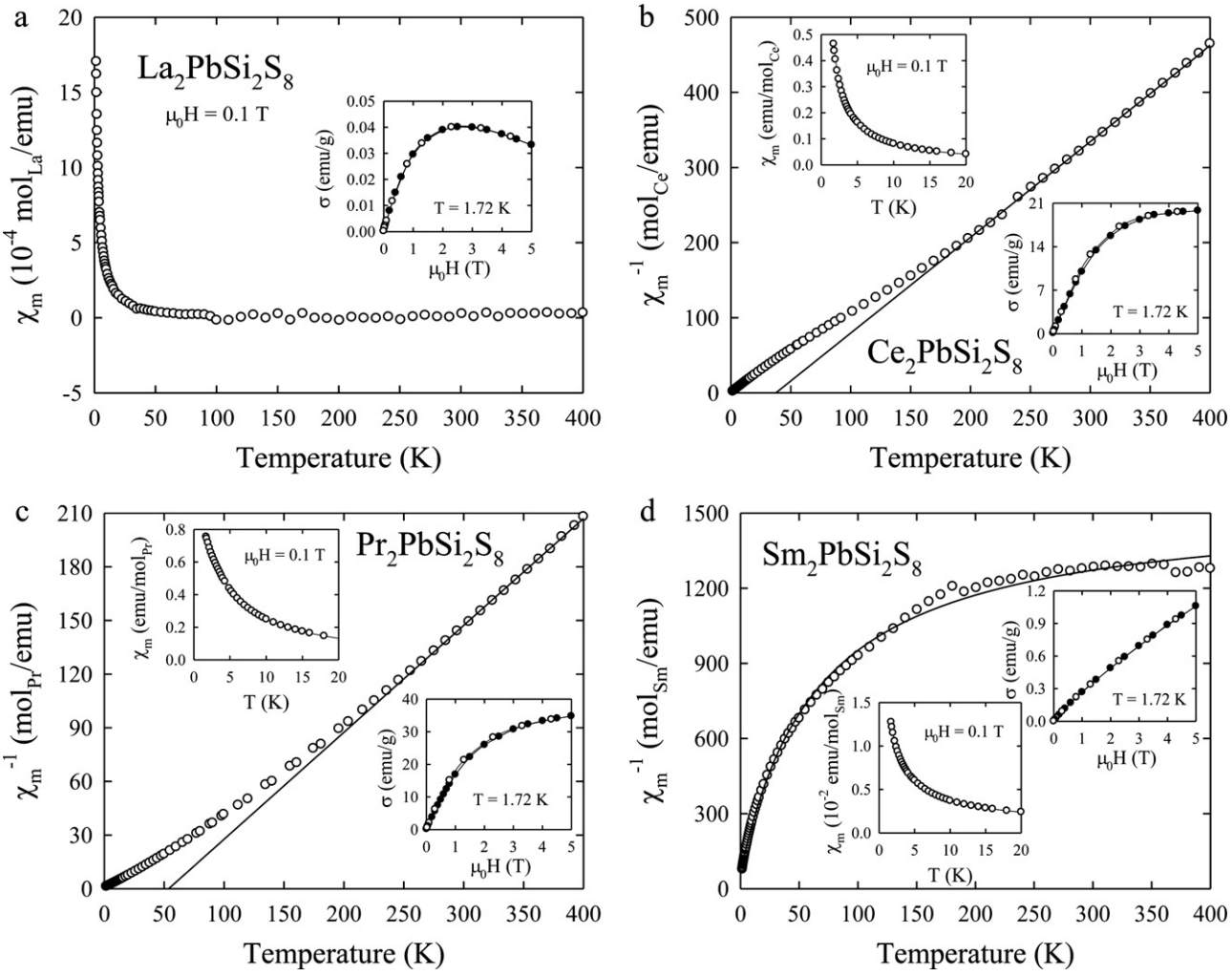

Fig. 3. (a) Temperature dependence of the molar magnetic susceptibility of $La_2PbSi_2S_8$. Inset: magnetic field variation of the magnetization in $La_2PbSi_2S_8$ taken at $T = 1.72$ K with increasing (full circles) and decreasing (open circles) field strength. (b and c) Temperature dependencies of the inverse molar magnetic susceptibility of $Ce_2PbSi_2S_8$ and $Pr_2PbSi_2S_8$. The solid lines denote the Curie–Weiss fits with the parameters given in the text. Upper insets: low-temperature dependencies of the molar magnetic susceptibility of $Ce_2PbSi_2S_8$ and $Pr_2PbSi_2S_8$. Lower insets: magnetic field variations of the magnetization in $Ce_2PbSi_2S_8$ and $Pr_2PbSi_2S_8$ taken at $T = 1.72$ K with increasing (full circles) and decreasing (open circles) field strength. (d) Temperature dependence of the inverse molar magnetic susceptibility of $Sm_2PbSi_2S_8$. The solid line represents the modified Curie–Weiss fit with the parameters given in the text. Lower inset: low-temperature dependence of the molar magnetic susceptibility of $Sm_2PbSi_2S_8$. Upper inset: magnetic field variation of the magnetization in $Sm_2PbSi_2S_8$ taken at $T = 1.72$ K with increasing (full circles) and decreasing (open circles) field strength.

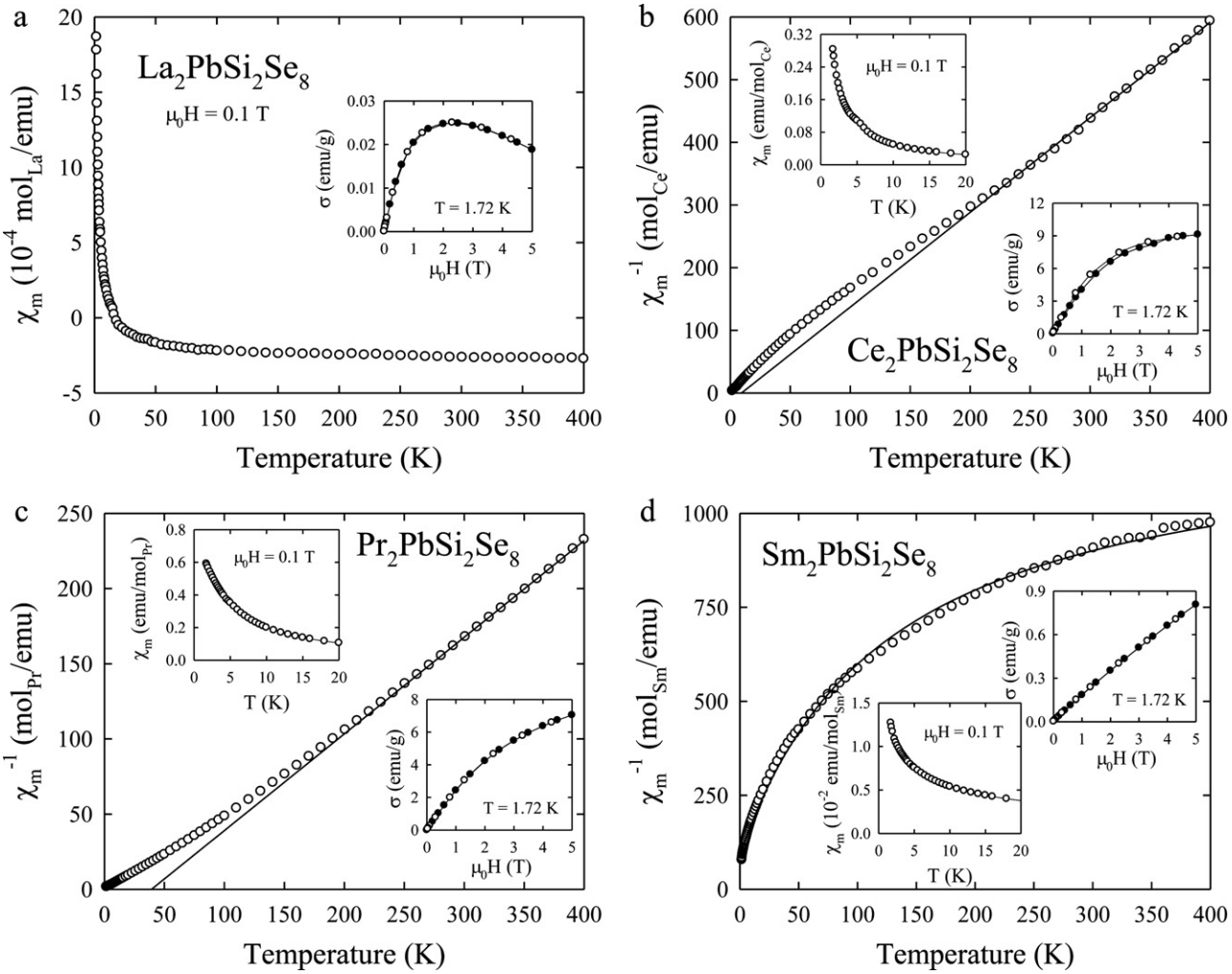

Fig. 4. (a) Temperature dependence of the molar magnetic susceptibility of $La_2PbSi_2Se_8$. Inset: magnetic field variation of the magnetization in $La_2PbSi_2Se_8$ taken at $T = 1.72$ K with increasing (full circles) and decreasing (open circles) field strength. (b and c) Temperature dependencies of the inverse molar magnetic susceptibility of $Ce_2PbSi_2Se_8$ and $Pr_2PbSi_2Se_8$. The solid lines denote the Curie–Weiss fits with the parameters given in the text. Upper insets: low-temperature dependencies of the molar magnetic susceptibility of $Ce_2PbSi_2Se_8$ and $Pr_2PbSi_2Se_8$. Lower insets: magnetic field variations of the magnetization in $Ce_2PbSi_2Se_8$ and $Pr_2PbSi_2Se_8$ taken at $T = 1.72$ K with increasing (full circles) and decreasing (open circles) field strength. (d) Temperature dependence of the inverse molar magnetic susceptibility of $Sm_2PbSi_2Se_8$. The solid line represents the modified Curie–Weiss fit with the parameters given in the text. Lower inset: low-temperature dependence of the molar magnetic susceptibility of $Sm_2PbSi_2Se_8$. Upper inset: magnetic field variation of the magnetization in $Sm_2PbSi_2Se_8$ taken at $T = 1.72$ K with increasing (full circles) and decreasing (open circles) field strength.

of the magnetic moments is another indication of the strong crystal field interactions in the materials studied.

As can be inferred from Figs. 3 and 4, the temperature variations of the inverse magnetic susceptibility of the two Sm-based phases are strongly curvilinear in the entire temperature range.

Table 5
Lattice parameters of the $R_2PbSi_2S_8$ (R = Y, Sm, Gd, Tb, Dy, Ho), $Pr_2PbGe_2S_8$ and $R_2PbSi_2Se_8$ (R = Sm, Gd) compounds.

Compound	a, Å	c, Å	V, Å^3	Calculated density, g/cm^3
$Y_2PbSi_2S_8$	8.8433(2)	25.9745(9)	1759.2(1)	3.944
$Sm_2PbSi_2S_8$	8.8854(4)	26.283(1)	1797.0(2)	4.545
$Gd_2PbSi_2S_8$	8.8633(6)	26.185(3)	1781.5(4)	4.663
$Tb_2PbSi_2S_8$	8.8604(1)	26.1184(7)	1775.76(9)	4.696
$Dy_2PbSi_2S_8$	8.8422(1)	26.0033(5)	1760.66(7)	4.777
$Ho_2PbSi_2S_8$	8.8428(2)	25.963(1)	1758.2(1)	4.812
$Pr_2PbGe_2S_8$	8.9840(2)	26.8670(9)	1878.0(1)	4.721
$Sm_2PbSi_2Se_8$	9.2620(4)	27.487(1)	2042.1(3)	5.830
$Gd_2PbSi_2Se_8$	9.2320(7)	27.329(3)	2017.2(5)	5.971

Such behaviour is typical for samarium compounds for which the terms $^6H_{5/2}$ and $^6H_{7/2}$ of the Sm^{3+} ground multiplet are close in energy [10]. To account for this character of $\chi^{-1}(T)$ one may apply the so-called modified Curie–Weiss (MCW) law, $x = C/(T-\theta)+x_0$, in which the Van Vleck contribution to the magnetic susceptibility is represented by the temperature-independent term χ_0. The parameters derived from least-squares fits of the MCW formula to the experimental data of $Sm_2PbSi_2S_8$ and $Sm_2PbSi_2Se_8$ are equal to $\mu_{eff} = 0.57\,\mu_B$/Sm-ion, $\theta = -3$ K, $\chi_0 = 7 \times 10^{-4}$ emu/(mol Sm-ion) and $\mu_{eff} = 0.87\,\mu_B$/Sm-ion, $\theta = -9$ K, $\chi_0 = 8 \times 10^{-4}$ emu/(mol Sm-ion), respectively. It is worth noting that the experimental value of μ_{eff} found for the selenide is very close to the effective magnetic moment predicted for a free Sm^{3+} ion in the framework of the Russell–Saunders approach ($g\sqrt{J(J+1)} = 0.84$), whereas that calculated for the sulphide is considerably smaller than the theoretical value. For both compounds, the paramagnetic Curie temperature is negative, as expected for systems with antiferromagnetic correlations. Nevertheless, as displayed in the insets in Figs. 3 and 4, the temperature-dependent magnetic susceptibility of $Sm_2PbSi_2S_8$ and $Sm_2PbSi_2Se_8$ is featureless down to the lowest temperature

studied. The absence of long-range magnetic ordering in these compounds is also apparent from the other insets in the respective panels, which present the magnetic field variations of the magnetization taken at 1.72 K. For both chalcogenides, the magnetization isotherms behave in a manner characteristic of Curie–Weiss paramagnets.

4. Conclusions

The formation of an extended series of quaternary compounds isostructural to $La_2PbSi_2S_8$ [4] has been established. These novel phases are the sulphides $R_2PbSi_2S_8$ (R = Y, Ce, Pr, Nd, Sm, Gd, Tb, Dy, Ho) and $R_2PbGe_2S_8$ (R = Ce, Pr), as well as the selenides $R_2PbSi_2Se_8$ (R = La, Ce, Pr, Nd, Sm, Gd). All these materials crystallize with the hexagonal unit cells, in which R and Pb atoms statistically share same position inside bi-capped trigonal prisms made by chalcogen atoms. The compounds $R_2PbSi_2S_8$ and $R_2PbSi_2Se_8$ with R = Ce, Pr and Sm exhibit strongly temperature dependent paramagnetic behaviour due to the presence of localized magnetic moments of trivalent rare-earth ions. For none of them any hint for long-range magnetic ordering has been found down to 1.72 K. The La-based materials are weak diamagnets, as expected for systems with no 4f electrons.

References

[1] V.A. Starodub, Usp. Khim. 68 (10) (1999) 883 (in Russian).
[2] K. Mitchell, J.A. Ibers, Chem. Rev. 102 (2002) 1929.
[3] L.D. Gulay, M. Daszkiewicz, in: K.A. Gschneidner Jr., J.-C.G. Bünzli, V.K. Pecharsky (Eds.), Handbook on the Physics and Chemistry of Rare Earths, Ternary and Quaternary Chalcogenides of Si, Ge, Sn, Pb, and In, vol. 41, 2011 (Chapter 250).
[4] L.D. Gulay, M. Daszkiewicz, I.P. Ruda, O.V. Marchuk, Acta Crystallogr. C66 (2010) i19.
[5] L.G. Aksel'rud, Yu.N. Grin', P.Yu. Zavalij, V.K. Pecharsky, V.S. Fundamensky, Collected Abstr. 12th Eur. Crystallographic Meet., Moscow, August 1989, vol. 3, Izv. Acad. Nauk SSSR, Moscow, 1989, p. 155.
[6] Oxford Diffraction, CrysAlis CCD and CrysAlis RED, Version 1.171.30.3, Oxford Diffraction Ltd., Abingdon, Oxfordshire, England, 2006.
[7] G.M. Sheldrick, SHELXS97 and SHELXL97, Programs for the Solution and the Refinement of Crystal Structures, University of Göttingen, Germany, 1997.
[8] A.L. Spek, PLATON, a Multipurpose Crystallographic Tool, Utrecht University, Utrecht, The Netherlands, 2007.
[9] N. Wiberg, Lehrbuch der Anorganischen Chemie, Walter de Gruyter, Berlin, 1995, pp. 1838–1841.
[10] K.N.R. Taylor, M.I. Darby, Physics of Rare Earth Solids, Chapman and Hall, London, 1972.